Session 4A (2) – Ultrasonics

Chairman – ***Dr C Brett***

14.45 Enhancing sizing resolution and off-axis flaw depth accuracy in D-scans using signal processing and mode-converted waves (under revision)

Authors - ***A. Al-Ataby, W. Al-Nuaimy and C. R. Brett***

The aim of this paper is to study the extent of the errors when the tip of a flaw is off-axis, i.e. when the flaw tip is positioned away from the central axis. Also, the paper shows how to use mode-converted waves as a method for the accurate determination of depth in such cases for a non-parallel scans (D-scans).

Enhancing sizing resolution and off-axis flaw depth accuracy in time-of-flight diffraction D-scans using curve fitting and mode-converted waves

A. Al-Ataby and W. Al-Nuaimy
Department of Electrical Engineering and Electronics, University of Liverpool
Liverpool, L69 3GJ, UK
Tel: +44 151 794 4580, Fax: +44 151 794 4540
aliataby@liv.ac.uk, wax@liv.ac.uk

Abstract

Despite the recent popularity of ultrasonic time-of-flight diffraction (TOFD) as a reliable non-destructive testing technique for the inspection of weld defects in steel structures, the critical stages of data processing and interpretation are still performed manually. This is subject to inevitable human errors due to reduced alertness arising from operator fatigue and visual strain when processing large volumes of data.

This paper presents techniques developed for accurate sizing and positioning of weld flaws in TOFD D-scan data as an essential stage in a comprehensive TOFD inspection and interpretation system to aid the operator by automating some aspects of the processing and interpretation. Data manipulation and post-processing techniques have been specifically developed for the sizing of weld defects in TOFD data, significantly reducing the sizing and positioning errors for off-axis flaws. The mode-converted waves are utilised to enhance positional accuracy of flaws. The results achieved so far have been promising in terms of accuracy, consistency and reliability.

1. Introduction

The pulse echo method in ultrasonic inspection relies on the echo amplitude to size the flaw and the pulse travel time to locate the defect position and orientation [(1)]. This method is based on the assumption that echoes from the planar features are suitably angled and travel back to the transducer. Though simple and inexpensive, it suffers from poor resolution for crack sizing when the echo may be severely attenuated because the amplitude of the reflected echo may be influenced by factors such as surface roughness, particles in the specimen, transparency and orientation of the flaw. To overcome the limitations of the pulse echo method, the ultrasonic TOFD was developed. It has higher accuracy for measuring the through-wall size of crack-like defects, and can be performed in a wide range of material thickness. It has gained popularity because of its high probability of detection, low false call rate, portability and most importantly, its intrinsic accuracy in flaw sizing and positioning, especially in depth [(1, 2, 3)].

2. Why size and position matter

Some flaws can very quickly be enlarged by fatigue and cause a major reduction of strength leading to catastrophic failure of the structure. This failure can occur by rapid brittle fracture if these flaws exceed a certain critical size for the load applied. In

practice, when a material is strained, energy is stored in the elastic displacement. If the material contains a crack, this stored strain energy is released by gradually increasing the size of the crack and brittle fracture can occur depending on the through-wall extent and orientation of the crack. Therefore, accurate measurement of the through-wall extent of the flaws has great importance in ensuring the structural integrity of many structures by detecting the defects that could trigger such a failure [3, 4]. Ultrasonic NDT techniques are commonly used to detect and size these flaws both pre-service and in-service. In the early use of pulse-echo ultrasonics, flaws could be detected but there was often little precision in flaw sizing, leading to some critical flaws not being detected and diagnosed correctly. Furthermore, this may lead to unnecessary repair or replacement of components, welded components in particular [4].

3. Off-axis depth error

3.1 Depth error calculation

In the D-scan configuration, the flaw is likely to be offset from the centre of the axis between the transmitter and receiver. However accurate the time of flight may be, the lateral position of the source of the echo is still unknown [4]. Consider the situation for a D-scan with the defect tip at depth d offset from the axis between the two probes by the distance X mm, and a transit time (neglecting probe delay) of t μs (Figure 1). The range for a signal from the defect tip is given by [3, 4]:

$$v_L t = \sqrt{(s+X)^2 + d^2} + \sqrt{(s-X)^2 + d^2} \quad \text{.....(1)}$$

where v_L is the longitudinal wave velocity in material.

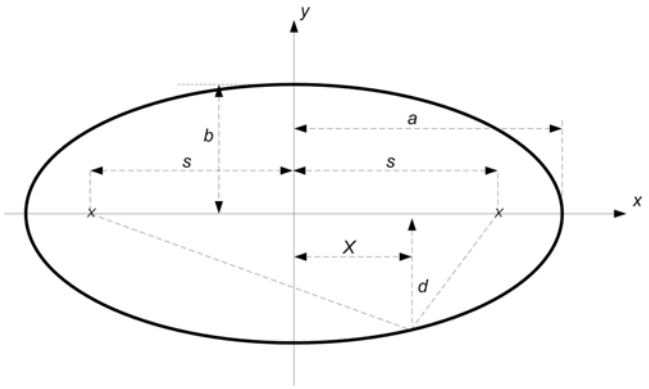

Figure 1. Ellipse with constant time-of-flight

The shape of the path with constant range (i.e. time) is an ellipse with the index points of the two probes at its foci. Rearranging Equation 1, the following expression for the depth d is obtained [3, 4]:

$$d = \sqrt{\left(\frac{1}{4} - \frac{X^2}{v_L^2 t^2}\right)\left(v_L^2 t^2 - 4s^2\right)} \quad \text{.....(2)}$$

This expression represents an ellipse with the beam entry points as foci and path length $v_L t$. From the equation it is clear that if X is unknown then d cannot be calculated. To overcome this problem, it is normal practice to perform a TOFD B-scan at the position of a detected defect to measure the depth accurately and find the offset X. Measurement errors are minimised because at some point within the B-scan the defect must lie equidistantly between the two probes. This operation requires that the operator first analyses the D-scan to find the locations of any potential flaws, and then carries out a number of supplementary B-scans to measure their depths. It is clear that this introduces a certain amount of subjectivity to the operation and adds to the total inspection time. However, this paper will show that this information can be obtained from the original D-scan.

In order to estimate the depth error for an off-axis crack tip, the maximum and minimum depth at which it could occur (i.e. d_{max} and d_{min}) need to be considered for a measured transit time (Figure 2).

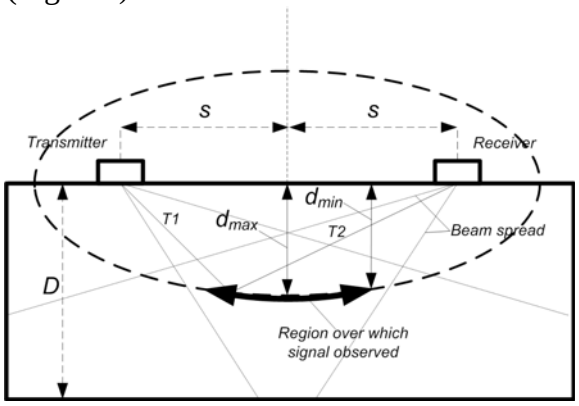

Figure 2. Uncertainty in lateral position in a D-scan

The maximum depth, d_{max}, is at the deepest point of the ellipse, i.e., when X=0, giving the familiar [4]:

$$d_{\max} = \sqrt{(v_L t/2)^2 - s^2} \quad \text{.....(3)}$$

According to the equation of the ellipse representing the path for transit distance $v_L t$, the minimum value for the depth, d_{min} is d=0 and consequently the term $(1/4\text{-}X^2/v_L{}^2t^2)$ must equal zero, i.e., $X = v_L t/2$. When d=0, the edge of the ellipse is beyond the probe and therefore represents an area not spanned by the probe and a defect in this position could not be observed since it lies outside the beam of the nearest probe. At the edge of the inspection coverage area, X is smaller than $v_L t/2$, i.e. a fraction f (where f <1/2). Thus, the ellipse position for d_{min} is when $X=fv_L t$, hence:

$$d_{\min} = \sqrt{(v_L{}^2t^2 - 4s^2)(1/4 - f^2)} \quad \text{.....(4)}$$

The maximum error expressed as a percentage of the maximum depth is given by:

$$d_{error} = \frac{d_{\max} - d_{\min}}{d_{\max}} = \frac{\left[(v_L t/2)^2 - s^2\right]^{1/2} - (v_L{}^2t^2 - 4s^2)^{1/2}(1/4 - f^2)^{1/2}}{[(v_L t/2)^2 - s^2]^{1/2}} \quad \text{.....(5)}$$

which is simplified to:

$$d_{error} = 1 - \sqrt{1 - 4f^2} \quad \text{.....(6)}$$

3.2 Variation of the depth error with off-axis distance

In practice, the lower edge of the acoustic beam determines the maximum detectable lateral position of a defect tip. If there is no information on the position of this edge then the maximum error could be at $X = s$. The variation of the fraction f with the offset distance X is quite complicated and the maximum value (at the edge of the beam) depends on the probe centre separation (PCS) and the probe parameters [5]. Take the typical situation of aiming the beam centres at $2D/3$, where D is the material thickness. Then, for an ellipse with depth $d=D/2$ (when the offset X is zero), the variation of the fraction f with offset distance X (expressed as a fraction of the distance s) is shown in Figure 3, and the corresponding percentage depth error d_{error} in Figure 4.

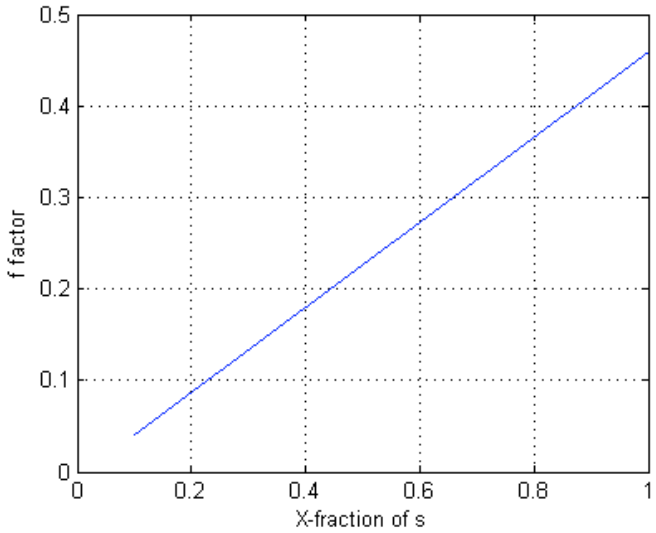

Figure 3. Variation of the factor *f* with off-axis distance *X* at *d* = *D*/2 and *s* = 2*D*/3 tan *θ* (*θ* is the probe angle)

The fraction f increases linearly with offset distance X from zero at X=0 to f=0.5 at $X = a$ (limit of ellipse $-v_L t/2$, Figure 1) while the depth error increasingly varies from zero at X=0 to about 70% at $X = a$. At the extreme position $X = s$ (i.e., defect is directly beneath one of the probes), f = 0.46 and the depth error is 60%. Thus, the depth error for an off-axis reflector can be very large [5].

Table 1 and 2 below show depth errors at the edge of the ultrasonic beam when the beam centres aimed at $2D/3$ and D of the sample, respectively, for a typical situation of a 60° probe, with 5 MHz and 6 mm crystal diameter, lower beam angle of 45° and for a beam edge cut-off of 10 dB [5].

4. Minimising the uncertainty in lateral position of off-axis flaws

4.1 Diffraction arcs

As mentioned earlier, in a D-scan configuration, the flaw is likely to be offset from the centre of the axis between the transmitter and receiver by a distance X as shown in Figure 5. By assuming, as current processing and reporting software invariably does, that the diffracted returns originate from a point mid-way between the transducers (i.e., $X = 0$) the interpreted depth suffers from an error. This error (Δd_X) due to the error in lateral position can be calculated by [3, 4]:

$$\Delta d_X = \frac{X^2}{v_L^2 t^2} \sqrt{\frac{v_L^2 t^2 - 4s^2}{\frac{1}{4} - \frac{X^2}{v_L^2 t^2}}} \quad \text{.....(7)}$$

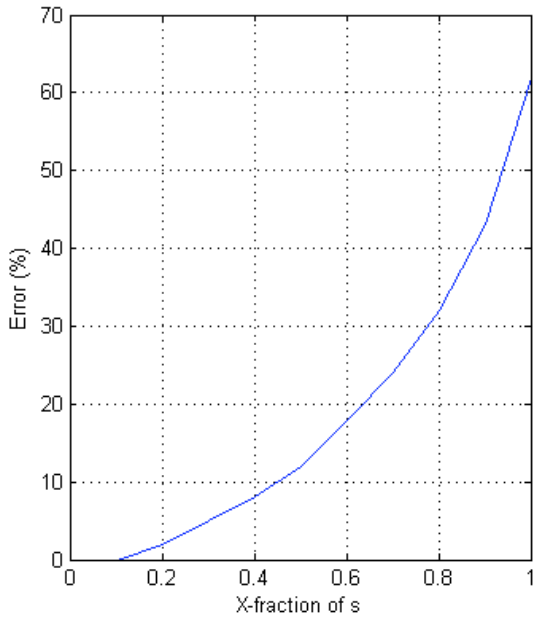

Figure 4. Variation of depth error with off-axis distance X at $d = D/2$ and $s = 2D/3 \tan \theta$ (θ is the probe angle)

Table 1. Depth errors at edge of the beam for $s = 2D/3 \tan 60^o$

Depth	f	Depth error (%) at beam edge
$D/2$	0.26	14.6
$2D/3$	0.18	7.0
D	0.05	0.5

Table 2. Depth errors at edge of the beam for $s = D \tan 60^o$

Depth	f	Depth error (%) at beam edge
$D/2$	0.34	27
$2D/3$	0.29	18.1
D	0.18	6.9

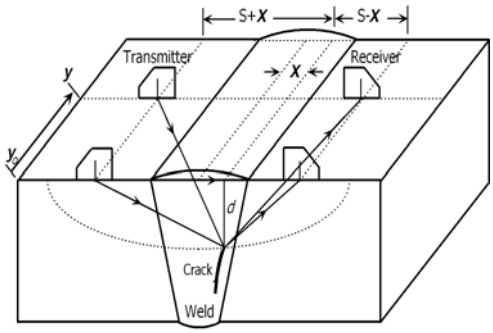

Figure 5. Effect of lateral flaw position on the arrival time in D-scan

Although flaw sizing using TOFD in D-scanning mode is more accurate than other conventional ultrasonic techniques, this depth error can still be of high order (as shown previously). When the flaw is located in the plane normal to the inspection surface and passing through both transmitter and receiver, the transit time of the pulse is at a minimum. As the transducers move away from this position as shown in Figure 5, along a scan line perpendicular to the plane of the flaw, the transit time increases resulting in ***arcs*** or ***wings*** at the ends of the flaw record in D-scan presentation. For a flaw located at a position y_o (in Figure 5) along the weld, the shortest path of a diffracted signal when the transmitter and receiver are moved to position y can be shown to be [4]:

$$v_L t = \sqrt{(s+X)^2 + d^2 + (y-y_o)^2} + \sqrt{(s-X)^2 + d^2 + (y-y_o)^2} \quad \text{.....(8)}$$

This equation represents the dependence of end of defect signature shape on the lateral offset X as shown in Figure 6. The depth error is directly related to X (follows from Equation 7) [3, 4].

4.2 Curve fitting

Equation 8 is recognised as the equation of a hyperbola for variables t and y. This has two branches; in the one of physical interest, t is at a minimum at the point where the scattering point lies in the plane defined by the two beam axes and it increases as the point moves away from that plane. From physical argument, it is clear that signal loci, although hyperbolic only in the special case referred to above, is of the same general shape for all scan paths in this simple geometry. In particular, the signal loci for a scan parallel to the plane defined by the beam axes will look very much like hyperbolas for deep defects but will appear increasingly flattened as the defect is approached [4].

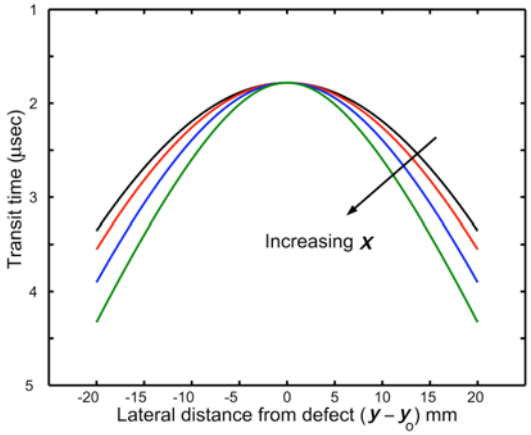

Figure 6. Dependence of defect signature shape on lateral offset *X* from defect

When the defect is well away from the beam axes of the transducers, even simple defects can yield complex patterns of arcs. These arise because signals generated at the separate transducer edges can travel to the defect and back to the receiver as distinct wavepackets without interference, making it appear as though for each pair of probes there were in fact two transmitters and two receivers giving four possible arcs for each defect extremity. These effects are only striking in the near field of the transducers.

Since the shape of the arcs depends only on the defect depth, the defect lateral displacement, probe separation and direction of probe motion, it is predetermined for any given depth on a B- or D-scan display. It is a simple matter to provide a means of displaying the correct shape as a cursor on a digital display and to allow it to be moved interactively to check its fit to any suspected defect indication.

For each detected defect, the edge points of the defect signature can be determined by a combination of 2-D alignment processing and 1-D peak tracing for each echo. As a result, the sets of points representing the envelope of the defect echo wavefront can be detected. These sets of points can be checked if they are arcs by identifying those with a monotonic increase in time. These points are then modelled to fit (curve fitting process), in a minimum mean square error sense, a curve governed by Equation 9 (following from Equation 8) with varying X from 0 to s and varying d from d_{min} to d_{max} possible values [4]:

$$t = \frac{1}{v_L}\left[\sqrt{(s+X)^2 + d^2 + (y-y_o)^2} + \sqrt{(s-X)^2 + d^2 + (y-y_o)^2}\right] \quad \text{.....(9)}$$

As a result of this curve fitting shown in Figure 7, not only X can be found but also the start point of the arcs can be identified more accurately. This point is then used to correct the measured width of the defect to eliminate the effect of elongation, while the estimated value of X is then used in Equation 2 to correct the lateral position of the defect and, hence, minimise the depth error which increases the accuracy of the sizing measurements [4, 6]. Figure 8 shows sample results after the application of the curve fitting method on sample defect types.

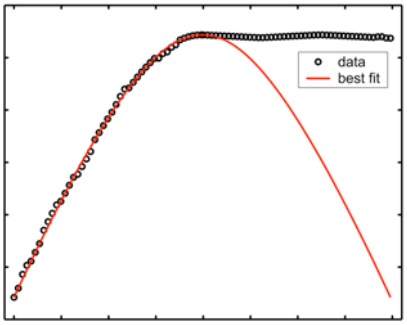

Figure 7. Extracting arc start point and fitting

5. Mode-converted waves and flaw position estimation

Section 4.2 has shown that it is possible to measure the transverse position of a defect when performing an ultrasonic TOFD D-scan by studying how the arcs (or wings) of a defect indication vary with scan position. This information would normally be obtained only from a B-scan image. One limitation that this method suffers from is that it does not indicate whether the defect is off-axis to the right or left of the weld (see Figure 9). In other words, the value of X is determined accurately, but it is not obvious whether this off-axis shift is to the left or to the right of the centre line of the weld.

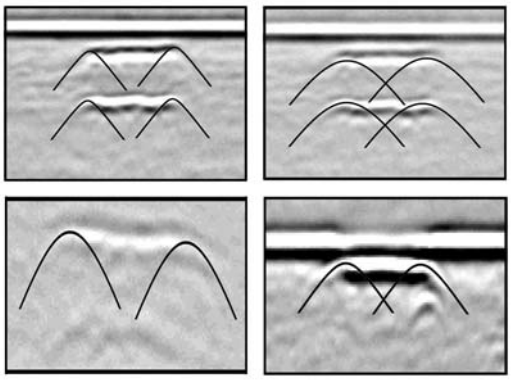

Figure 8. Representation of curve fitting method on sample defect types

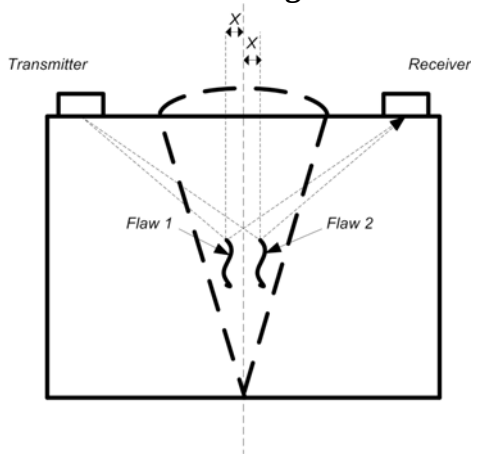

Figure 9. The two possible positions of a flaw when it is offset from centre line

To overcome this limitation, mode-converted waves can be used. Basically, each defect shows an indication in the mode-converted region of the scan that is usually more visible and indicative (because shear waves are twice as sensitive as transverse waves, having shorter wavelength and a lower velocity). In case of uncertainty in deciding the position of the off-axis flaw by interpreting the indication in the compression-to-shear wave region, then the time of the mode-converted indication can be used. Figure 10 shows this concept. By checking the time difference between defects in the mode-converted part of the D-scan display, the flaw can be concluded to be either closer to the transmitter or the receiver of the scanning equipment.

Most of the equipment used for TOFD scanning can provide the facility of operating multichannel probes concurrently (called software channels). Using this feature (and referring to Figure 11), the channels are defined as follows:

- Channel 1: Probe 1 is transmitting, probe 2 is receiving.
- Channel 2: Probe 1 is receiving, probe 2 is transmitting.

As it can be seen from Figure 11, the indication in the compression region shows almost the same position for both transmitter-receiver setups. The difference can be seen in the mode-converted region, where there are two different times (t_1 and t_2) for the same defect depending on probes setup. Obviously, the flaw is actually closer to R_1 in the T_1-R_1 setup (shortest time is more accurate). By utilising these observations in conjunction with the method explained in Section 4.2, accurate sizing and positioning measurements were achieved.

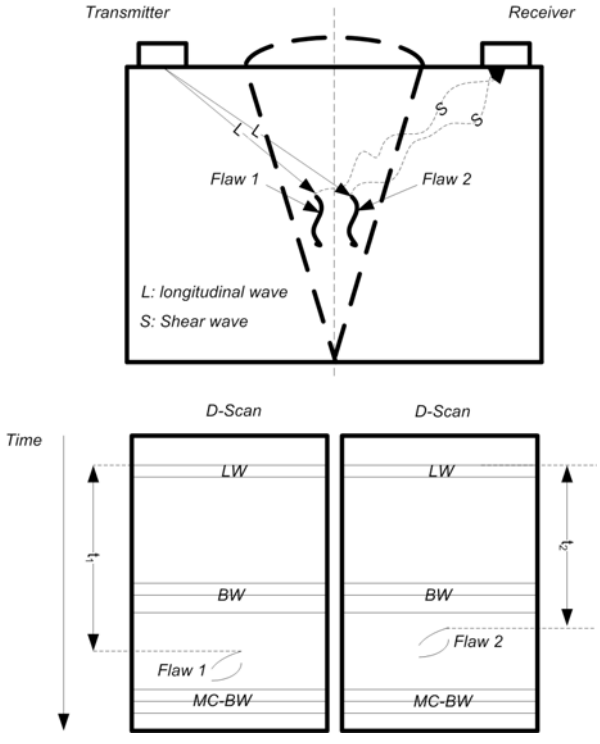

Figure 10. Time difference between defects in the mode-converted indication ($t_2 < t_1$, then flaw 2 is closer to the receiver)

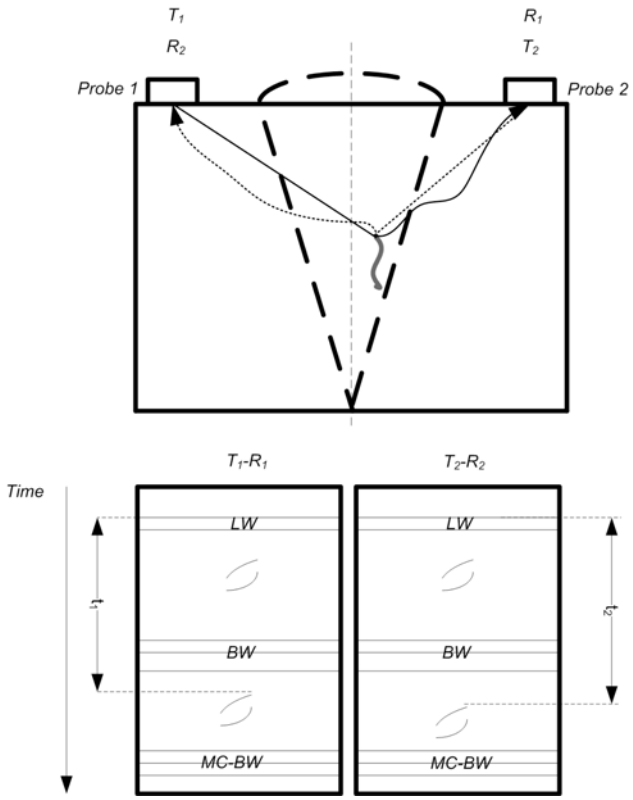

Figure 11. The flaw is actually closer to R_1 in T_1-R_1 setup (shortest time)

6. Results

The developed procedures have been applied to a data set consisting of 76 D-scans and containing 150 weld defects. These defects have all been characterised and documented by the manufacturer of the steel plates.

The majority of the achieved preliminary results are more accurate than the manual results, referring to the data sheets of the scanned plates, while only around 11% are the same as reported by a trained operator. For flaw depth measurements, the error is within ±1 mm, for all defect classes except for the surface breaking crack where the error is within ±2 mm because the flaw echo is merged with the lateral wave or backwall echo. For flaw height measurements, the error is within ±1mm for all defect classes except for the surface breaking crack where the error is within ±3 mm. For flaw width measurements, the error in the majority of cases is within ±1mm, but for some cases it is within ±3 mm.

7. Conclusions

This paper has addressed the task of accurate sizing and positioning of detected defects in ultrasonic TOFD data as part of a comprehensive automatic interpretation aid. Data manipulation and post-processing techniques have been developed to enhance sizing and positioning accuracy as compared to the accuracy obtained by human interpretation through an expert operator.

Results of the application of these techniques to the available data have been extremely promising in terms of speed, robustness, accuracy and reliability when dealing with highly variable data. This would make the proposed system suitable for implementation in situations requiring near real-time processing and interpretation of large volumes of data, and thus these techniques are expected to greatly reduce the possibility of human and experimental error, due to loss of concentration and visual fatigue, and the reliance on intervention from a trained operator, and could potentially open a new paradigm in TOFD for automatic interpretation. The utilisation of the mode-converted waves in accurate sizing looked very promising and is under thorough investigation to expand its added value.

Acknowledgements

The authors would like to express their gratitude and appreciation to E.ON Engineering Technology Centre for their support and funding of this work, and also to Tim Armitt of Lavender International NDT for providing access to the TOFD data acquisition systems.

References

1. M G Silk, ‘Defect sizing using ultrasonic diffraction’, British Journal of NDT, pp 12-15, January 1979.
2. A Al-Ataby, W Al-Nuaimy, C R Brett and O Zahran, ‘Automatic detection and classification of weld flaws in TOFD data using Wavelet transform and support vector machines’, The BINDT Conference, Blackpool, September 2009.
3. J Charlesworth and J Temple, ‘Engineering applications of ultrasonic time-of flight diffraction’, RSP, 2nd edition, 2001.
4. A Al-Ataby, O Zahran, and W Al-Nuaimy, ‘Towards automatic flaw sizing using ultrasonic time-of-flight diffraction’, Insight, Vol 52, No 7, pp 336-371, July 2010.
5. British Standards Institution, ‘Guide to calibration and setting-up of the ultrasonic time of flight diffraction (TOFD) technique for the detection, location and sizing of flaws’, BS 7706, December 1993.
6. M G Silk, ‘An evaluation of the performance of the TOFD technique as a means of sizing flaws, with particular reference to flaws with curved profiles’, Insight, Vol 38, No 4, pp 280-287, April 1996.